Glider Observations of the Northwestern Iberian Margin During an Exceptional Summer Upwelling Season

Callum Rollo[1], Karen J. Heywood[1], Rob A. Hall[1], Eric Desmond Barton[2], Jan Kaiser[1]

[1]Centre for Ocean and Atmospheric Sciences, School of Environmental Sciences, University of East Anglia, Norwich, United Kingdom

[2]Instituto de Investigaciones Marinas (CSIC), Vigo, Spain

Key Points:

- A glider observed two upwelling events during a 70 day deployment over the Northwestern Iberian Margin in summer 2010.
- During upwelling decreasing temperature and increasing chlorophyll a concentration lead increasing dissolved oxygen concentration by 6 days.
- Equatorward flow persisted over the shelf and upper slope throughout the deployment.

Corresponding author: Callum Rollo, `c.rollo@uea.ac.uk`

Abstract

Glider observations from the Northwestern Iberian Margin during the exceptionally strong 2010 summer upwelling season resolved the evolution of physical and biogeochemical variables during two upwelling events. Upwelling brought low oxygen Eastern North Atlantic Central Water from 190 m depth onto the shelf up to a depth of 50 m. During the two observed periods of upwelling, a poleward jet developed over the shelf break. The persistent upwelling favourable winds maintained equatorward flow on the outer shelf for two months with no reversals during relaxation periods, a phenomenon not previously observed. During upwelling, near surface chlorophyll a concentration increased by more than 6 mg m^{-3}. Oxygen supersaturation in the near surface increased by more than 20 %, 6 days after the chlorophyll a maximum.

Plain Language Summary

In summer 2010, an autonomous underwater vehicle was used to measure changing water properties in the ocean offshore of Vigo, NW Spain. During summer, winds blowing southward along the Iberian coast push surface waters offshore, causing deep, cold, nutrient rich water to rise to the surface. The nutrients brought up with this cold water enable growth of phytoplankton, impacting higher trophic levels and local fisheries. During June and July 2010 we observed two episodes of deep water rising and the subsequent increases in phytoplankton. Increases in dissolved oxygen concentration and ocean current speed were also observed. Using a robotic underwater glider allowed us to obtain high resolution observations over a longer time period at a fraction of the cost of a research vessel cruise.

1 Introduction

Eastern Boundary Upwelling Systems are some of the oceans' most productive areas, covering less than 1 % of the ocean but accounting for up to 20 % of the global wild fish take (Pauly & Christensen, 1995). The Northwestern Iberian Margin (NWIM) forms the northernmost extent of the Canary Current Upwelling System, an Eastern Boundary Upwelling System of the North Atlantic. The NWIM hosts a seasonally varying multicore flow that exhibits strong variability (Teles-Machado et al., 2015). With the northward movement of the Azores High and the intensification of the Icelandic Low in summer, episodic southward winds blow along the Iberian coastline (Peliz et al., 2002; Nolasco et al., 2013). These southward winds drive warm surface waters offshore by Ekman transport, inducing the upwelling of cooler, nutrient rich water from as deep as 200 m and enhancing local primary production (Barton, 2001). During upwelling periods, typically 7-10 days (Huthnance et al., 2002; Ferreira Cordeiro et al., 2018), the coastal sea level lowers, the thermocline rises and an equatorward coastal jet develops over the shelf (Arístegui et al., 2009).

The NWIM extends 350 km along the west coast of the Iberian peninsula, from Cape Mondego to Cape Finisterre (Figure 1). The NWIM consists of a shelf 50-60 km wide that slopes gently to the shelf break between the 200 and 300 m isobaths before dropping to 2000 m over a distance of 15 km. The glider deployment area, in the neighbourhood of Cape Silleiro, is known to feature intensified upwelling in summer (Huthnance et al., 2002; Relvas et al., 2007). The shelf and slope region host seasonally varying meridional flows detailed by Herrera et al. (2008); Ferreira Cordeiro et al. (2018). Offshore, the North Atlantic subtropical gyre transports water equatorward in the broad, slow Portugal Current (Arístegui et al., 2009). The most variable current over the slope is the Iberian Poleward Current (IPC). The IPC transports water poleward, primarily driven by meridional density gradients (Peliz, 2003). During summer, this poleward flow coexists with two equatorward flows, the Upper Slope Equatorward Current, a topographically steered jet along the slope, and the intermittent Upwelling Jet that transports shelf waters equatorward (Ferreira Cordeiro et al., 2018).

Three water masses are typically observed in the upper 1000 m over the NWIM. In the deeper waters over the slope, Mediterranean Water (MEDW) is observed, typically below 550-600 m (Fiuza et al., 1998; van Aken, 2000). Above the MEDW two modes of Eastern North Atlantic Central Water (ENACW) are distinguishable; the subpolar ($\mathrm{ENACW_{sp}}$) and subtropical ($\mathrm{ENACW_{st}}$) modes (Ríos et al., 1992). The two converge in the vicinity of Cape Finisterre around 42-44 °N (Peliz et al., 2002) and are approximately divided along $\sigma_\theta = 27.1$ kg m^{-3}. The overlying $\mathrm{ENACW_{st}}$ is warmer, saltier and more oxygen rich than $\mathrm{ENACW_{sp}}$, as has been observed elsewhere in the north east Atlantic (Damerell et al., 2016; Ferreira Cordeiro et al., 2018; Hall et al., 2017). $\mathrm{ENACW_{sp}}$ is typically observed from depths of 550-600 m up to 250-180 m. $\mathrm{ENACW_{st}}$ is observed higher in the water column, from 250 m to 20-70 m where it mixes with warm, brackish outflow of the Rías Baixas estuarine inlets to form the surface waters of the upper 20-70 m. These light surface waters flow offshore past the shelf break. The surface wa-

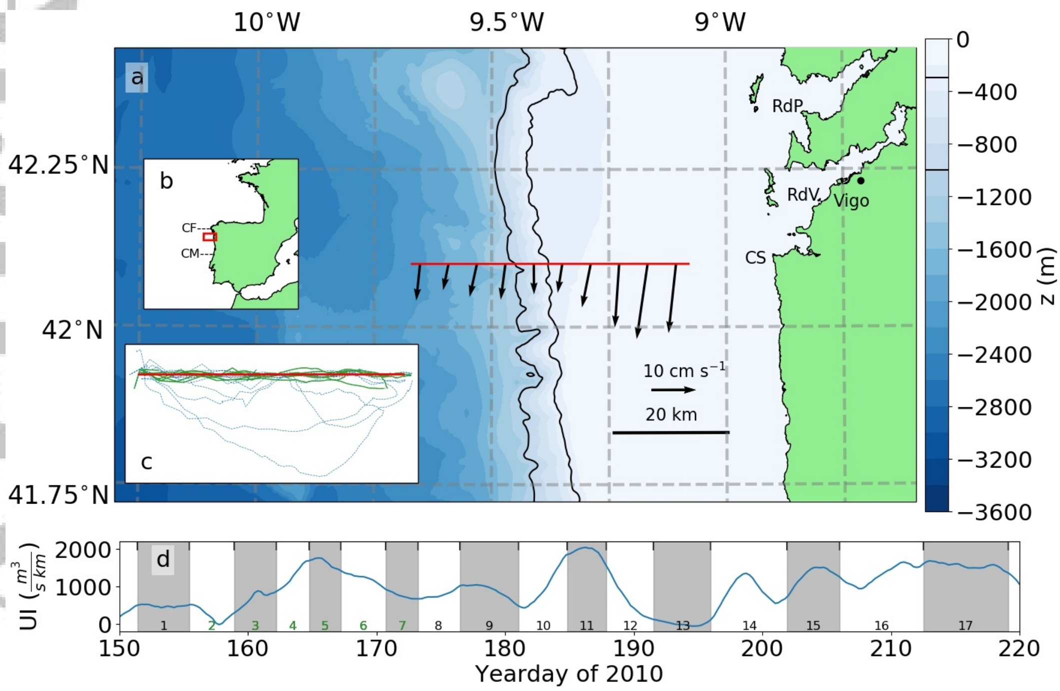

Figure 1. (a) Location of the glider section offshore of Vigo, NW Spain. Grey dashed lines at 1/4 degree intervals. Black lines demarcate the 300 and 1000 m isobaths, the shelf break and maximum profiling depth of the glider respectively. Red line marks the glider's nominal section. Arrows are the detided dive average currents, averaged over the deployment. Cape Silleiro is marked with CS. The mouths of the two southern Rías Baixas estuaries are marked: the Ría de Pontevedra (RdP) and Ría de Vigo (RdV). Bathymetry from the EMODnet Bathymetry Consortium (2018). (b) Limits of the Northwestern Iberian Margin, Cape Finesterre (CF) in the north and Cape Mondego (CM) in the south. Red box is area shown in (a). (c) Track of the glider during its 17 transects of the section, same scale as (a). Glider's nominal section in red. Green lines are transects 2-7. (d) Upwelling Index (UI) calculated with winds from the FNMOC model over yeardays 150-220 (30 May to 9 August) 2010. Shading shows the timing of the 17 numbered glider transects. Background shading indicates the direction of glider travel (grey: westward transects, white:eastward transects).

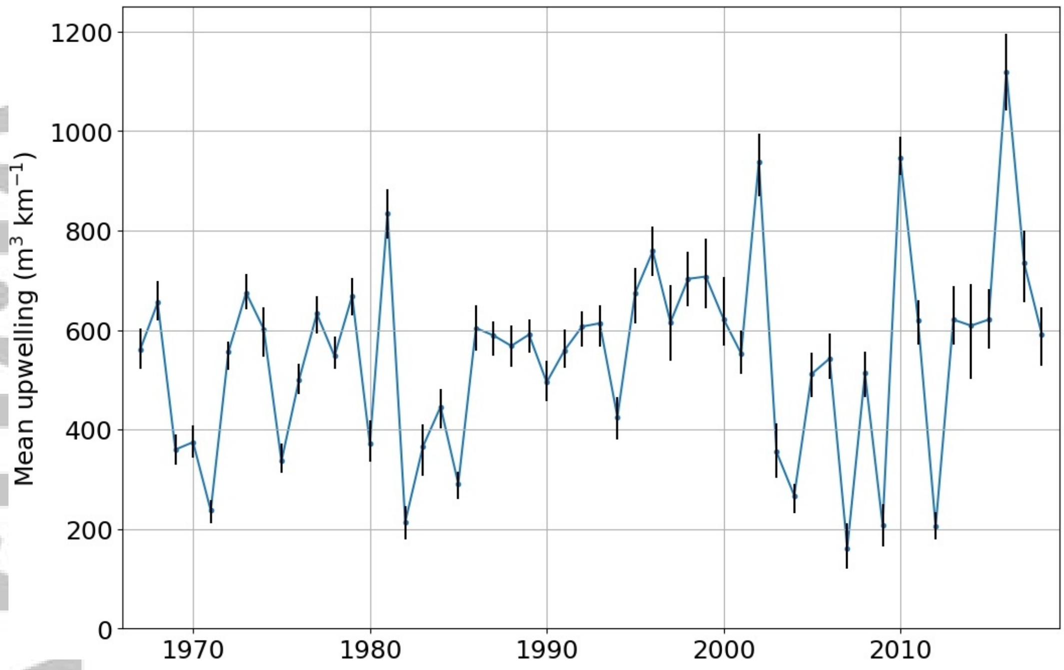

Figure 2. Mean and bootstrapped uncertainty range of the Upwelling Index for the 70 day interval 30 May to 8 August inclusive of each year.

ters are the warmest and most highly oxygenated waters of the NWIM. In summer, much of the vertical displacement of these water masses is driven by upwelling events (Álvarez-Salgado et al., 2000).

Upwelling episodes boost productivity along the shelf break, increasing primary production by up to 50 % compared with open ocean values (Joint et al., 2002). Due to upwelling, the NWIM hosts high concentrations of zooplankton and pelagic fish, enhancing its biological and economic importance (Rossi et al., 2013). During upwelling events, substantial cross-shelf exchange can take place (Brink, 1998). These events of enhanced primary productivity and offshore transport are the focus of this study.

The 2010 summer upwelling season was unusually strong. Winds originated from the direction 0±45° (i.e. within 45° of north) for 82 % of the deployment. The mean wind speed was 8.2 m s^{-1} and the mean Upwelling Index (UI) was 950 (± 40) m^3 km^{-1} s^{-1}. UI is an estimate of offshore Ekman transport. A positive value of UI is indicative of upwelling favourable conditions. UI for the region for each year over the same yearday range averaged 550 (± 190) m^3 km^{-1} s^{-1} (Puertos del Estado, 2019). In 2010, UI was two standard deviations above the mean (Figure 2). Similarly strong upwelling conditions occurred during 1981, 2002 and 2016. These unusually strong conditions resulted in a summer dominated by upwelling.

To observe this variability during the upwelling season at high spatial and temporal resolution, an autonomous ocean glider was deployed at the NWIM during summer 2010. The deployment is described in Section 2.1. Data processing and gridding are presented in Section 2.2. In Section 3 we present the results, in Section 4 we discuss the results and make recommendations for future observational campaigns on the NWIM. In Section 5 we summarise the key results.

2 Data collection and processing

2.1 Data collection

From 1 June to 5 August 2010, Seaglider SG510 Orca occupied an onshore-offshore section at 42.1 °N across the shelf and slope from 9.1 to 9.7 °W (Figure 1). Each passage through the section is referred to as a transect. Seagliders are small, buoyancy-powered vehicles that profile to 1000 m with a sawtooth dive pattern (Eriksen et al., 2001). The glider profiled over bathymetry of 150 to 2000 m. Individual dive cycle duration varied from 30 minutes on the shelf to 4 hours over the deep slope. During a dive the glider travels between 500 m and 4 km horizontally. Each dive cycle yielded two profiles, one when the glider was descending, one when it was ascending. The glider recorded measurements every 5 s above 200 m and every 10 s below 200 m. The glider has a typical vertical speed of 0.1 m s^{-1}, resulting in vertical sampling resolutions of approximately 0.5 m and 1.0 m respectively. The glider travelled zonally at 0.1-0.3 m s^{-1} relative to the ground.

The glider was equipped with a Paine Corporation pressure sensor, an unpumped Seabird CT sail, a WETLabs ECO Puck triplet sensor and an Aanderaa 4330F oxygen optode. Transects covered on average 45 km and took 2-6 days. Transect time increased towards the end of the deployment due to biofouling that increased drag on the glider (Figure 1d). The glider completed the section 17 times. Some transects were truncated but all were greater than 36 km (Figure 1c). Due to strong equatorward currents, the glider deviated meridionally from its intended zonal track with a standard deviation of 2.8 km (Figure 1c). Considering these deviations to be small, we have projected all samples onto a zonal section. We compared the temperature-salinity characteristics of all transects (not shown). Transects all sample the same water masses, even those with large meridional deviations. Transects 2 and 6 have been chosen as typical examples of non-upwelling and upwelling conditions respectively. Transect 2 took place after a period of relaxation favourable conditions, whereas transect 6 was conducted at the peak of the first upwelling event.

The shelf break is defined as the 300 m isobath shown in Figure 1. Throughout the text, "shelf" refers to waters east of the shelf break, "slope" refers to waters west of the shelf break. Yeardays (YD) are used throughout, with January 1st 2010 as yearday 0. The first day of this deployment 1 was June 2010, yearday 151.

2.2 Data processing and gridding

The hydrodynamic flight model for the glider was tuned following the methods of Frajka-Williams et al. (2011). Dive average currents (DACs) were calculated from the difference between the glider's flight path calculated from GPS fixes at the beginning and end of each dive, and the glider's flight path from the flight model. The flight model regression is very sensitive to drag coefficients, which varied greatly over the glider deployment. Parasitic drag increased by over 200 % due to biofouling. To accommodate this, the glider flight model was calculated using batches of 30 dives, allowing the friction coefficients to vary over the 1050 dives analysed. The DACs were inspected for directional biases that can arise from a poorly calibrated compass, but no substantial differences were found. Thermal lag of the CT cell was corrected following Garau et al. (2011). These corrections were implemented with the UEA Seaglider Toolbox (Queste, 2014).

To remove tidal currents from the DAC time series, dives were separated into two subsets, onshore and offshore of the shelf break, following the method of Sheehan et al. (2018) who separated DACs into three spatial bins for tidal analysis. These two datasets, each comprising approximately one month of DAC observations, were treated as discontinuous time series and harmonic analysis was used to extract the M_2 and S_2 tidal constituents. The combined $M_2 + S_2$ tidal current had a maximum amplitude of 0.5 cm s^{-1} over the slope and 2.0 cm s^{-1} on the shelf. The tidal constituents were validated against the TPXO tide model (Egbert & Erofeeva, 2002). The choice of two domains was made as the M_2 tidal component in the region varies substantially between shelf and slope (Quaresma & Pichon, 2013). Each bin also satisfies the Rayleigh criterion for distinguishing between the M_2 and S_2 tides with time series of greater than 14.8 days (Sheehan et al., 2018).

For the purposes of this paper, DAC is assumed to be an approximate barotropic current where the glider sampled the full water column and an approximate vertical average current in the upper 1000 m, where the bathymetry exceeded the glider's profiling depth. The M_2 and S_2 tidal constituents were subtracted from the DACs before using the DACs to reference geostrophic shear. DACs are typically considered accurate to within 1 cm s^{-1} (Eriksen et al., 2001; Merckelbach et al., 2008). Acknowledging that this detiding will not remove all tidal constituents from the DACs, we have incorporated a 2 cm s^{-1} uncertainty in our calculations of geostrophic currents. This uncertainty in geostrophic velocity is used for uncertainty estimates in alongshore transports.

The WETlabs ECO Puck measures fluorescence as a proxy for chlorophyll *a* concentration (henceforth chlorophyll). The ECO Puck excites chlorophyll by emitting at 470 nm and records florescence at 695 nm. Chlorophyll fluoresces at a range of wavelengths centred on 682 nm (Maxwell & Johnson, 2000). The chlorophyll florescence data are calculated using a linear equation $y = m(x-c)$, where y is chlorophyll concentration (mg m^{-3}) and x is the sensor output (counts). We used the manufacturer supplied gradient $m = 0.121$ and a dark counts level $c = 48$, 8 % lower than the manufacturer supplied value, such that the sensor registered 0 chlorophyll at depths greater than 150 m. An in-water calibration was carried out with co-located CTD casts on 1 June (YD 151), 29 June (YD 179) and 29 July (YD 210) (Brown, 2013). Chlorophyll values were corrected for the effects of non-photochemical quenching following the methodology of Thomalla et al. (2018). As the principal interest of this study is the cross shelf and temporal variability of chlorophyll, we are not aiming for an approximation of chlorophyll concentration better than a factor of two.

The Aanderaa optode is a low power foil type sensor as described by Alkire et al. (2012). Dissolved oxygen concentration was calculated using manufacturer calibration constants. The oxygen concentration was then corrected for temporal drift by applying a linear correction in time such that oxygen concentrations at 850-950 m depth remained constant in time. Winkler bottle samples were used to calibrate the ship CTD O_2 sensor on 29 July (YD 210), 15 September (YD 257) and 29 September (YD 271). This calibration was applied to CTD casts on 1 June (YD 151), 29 June (YD 179) and 29 July (YD 210) (Brown, 2013).

Temperature and salinity data for each transect were interpolated with an Objective Analysis Barnes function (Barnes, 1994) onto a grid with spacing 1 km horizontal by 1 m vertical, using a horizontal smoothing distance of 8 km and vertical smoothing of 8 m. This horizontal distance was chosen as it is the first internal Rossby radius of deformation over the shelf slope at the middle of the section. These gridded values were then used to calculate the potential density, absolute salinity and conservative temperature using the Gibbs Seawater toolbox (IOC & IAPSO, 2010). We found the geostrophic velocity field calculated from these interpolated data to be largely insensitive to smoothing distances from 0.5 to 15 km. Dissolved oxygen concentration and chlorophyll concentration were gridded using the same methodology.

Hovmöller plots were constructed by a Barnes interpolation of samples taken within $\pm$ 2.5 m vertically of the plot level. These samples were interpolated to a grid spaced 1 km horizontally and 8 hours in time, using a smoothing distance of 8 km and smoothing time of 3 days. This smoothing time was chosen as it is the typical response time of the NWIM to changes between upwelling and downwelling states (McClain et al., 1986).

Geostrophic currents were calculated from thermal wind, using the detided glider DACs as a reference velocity. The geostrophic approximation is commonly used with glider datasets in upwelling regions (Todd et al., 2011; Pietri et al., 2013), with estimated uncertainties of 1 -2 cm s^{-1}. Geostrophic currents calculated with this method compare well with ADCP data (Pietri et al., 2013). Bottom velocities were nearest neighbour extrapolated to fill gaps between glider sampling and bathymetry over the shelf and slope, with no extrapolation past the maximum measurement depth (1000 m). A Monte Carlo method was used to estimate uncertainty in the alongshore transports by applying random Gaussian noise with a standard deviation of 2 cm s^{-1} to the DACs, the largest source of error in estimation of geostrophic currents from glider data.

UI for the Rías Baixas is calculated by the Puertos del Estado at 6 hour intervals using the FNMOC model (Puertos del Estado, 2019). Satellite sea surface temperature (SST) from CMEMS Atlantic European North West Shelf Seas - Reprocessed SST Analysis - ODYSSEA from AVHRR Pathfinder v5.3, daily product 0.04 degrees resolution. Chl a satellite data from MODIS (Hu et al., 2012), daily product 0.0104 degree resolution. Bathymetry from EMODnet is used in this study (EMODnet Bathymetry Consortium, 2018).

We use units of conservative temperature and absolute salinity following IOC and IAPSO (2010). All densities are potential density anomalies σ_θ = potential density - 1000 with units of kg m^{-3}. Oxygen supersaturation, $\Delta(O_2)$ is calculated as

$$\Delta(O_2) = \frac{c(O_2)}{c_{eq}(O_2})) - 1, \tag{1}$$

where $c(O_2)$ is the measured O_2 concentration and $c_{eq}(O_2)$ is the O_2 concentration at an absolute pressure of 101325 Pa, calculated with potential temperature and salinity (Garcia & Gordon, 1992, 1993). A positive value represents oxygen supersaturation, a negative one represents oxygen undersaturation.

3 Results

3.1 Initial Conditions

Prior to upwelling (Figure 1d transects 1, and 2), conditions across the section were typical of relaxation. Isopycnals were near horizontal, with a plume of warm > 18 °C, low salinity < 35.9 g kg^{-1}, low density σ_θ < 26.0 kg m^{-3} water occupying the upper 20 m over the shelf and slope (Figures 3c, 4a and 4b). Vertical chlorophyll and $\Delta(O_2)$ distributions were similar across the section, with a subsurface chlorophyll maximum of 2.1 mg m^{-3} at 38 m and a $\Delta(O_2)$ maximum of 12 % from the surface to 25 m (Figures 5a and 5b). Water above the σ_θ = 26.9 kg m^{-3} isopycnal was supersaturated in oxygen, water below this isopycnal was undersaturated. The greatest chlorophyll concentrations and greatest $\Delta(O_2)$ were at the eastern end of the section, over the shelf. Below the pycnocline $\Delta(O_2)$ was greater over the shelf break and lower over the inner shelf, particularly near the sea floor where $\Delta(O_2)$ of less than -16 % was observed (Figure 5b).

During transects 3 and 4 (8-14 June), increasing wind speeds mixed the surface waters, increasing the mixed layer depth from 5 to 15 m (Figure 4). Chlorophyll in the upper 30 m increased by 0.8-1.6 mg m^{-3} and the subsurface chlorophyll maximum shoaled to 27 m (Figure 5c). After transect 4, the subsurface $\Delta(O_2)$ maximum was not observed. Wind speed increased to 13 m s^{-1} during transect 4.

3.2 First upwelling event

The first upwelling event began on 14 June (YD 164, Figure 6). This occurred during transects 4-7 of the deployment (Figures 4 and 5). The onset of upwelling was first

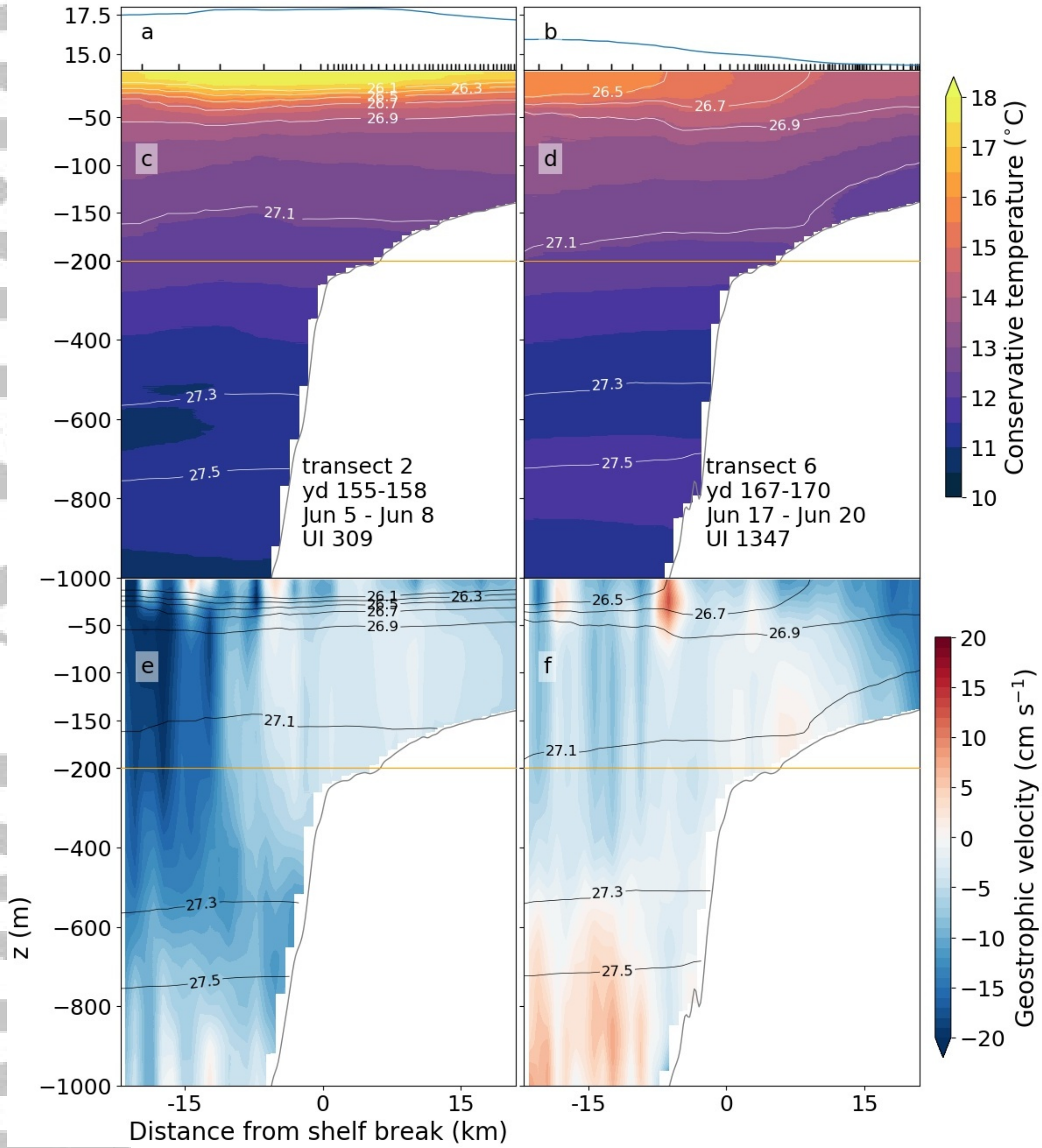

Figure 3. Conservative temperature (a-d) and meridional velocity (e & f). (a & b) Conservative temperature averaged over the uppermost 5 m, black ticks mark the surfacing of the glider during the transect for that column. (e & f) Meridional geostrophic velocity, negative velocity is equatorward. Density plotted with black lines. (a,c,e) Transect 2. (b,d,f) Transect 6. Density isopycnals mark the approximate boundaries between ENACW$_{st}$ and ENACW$_{sp}$ (σ_θ = 27.1 kg m^{-3}) and between ENACW$_{sp}$ and MEDW (σ_θ = 27.3 kg m^{-3}). Note that the vertical scale changes at z = -200 m.

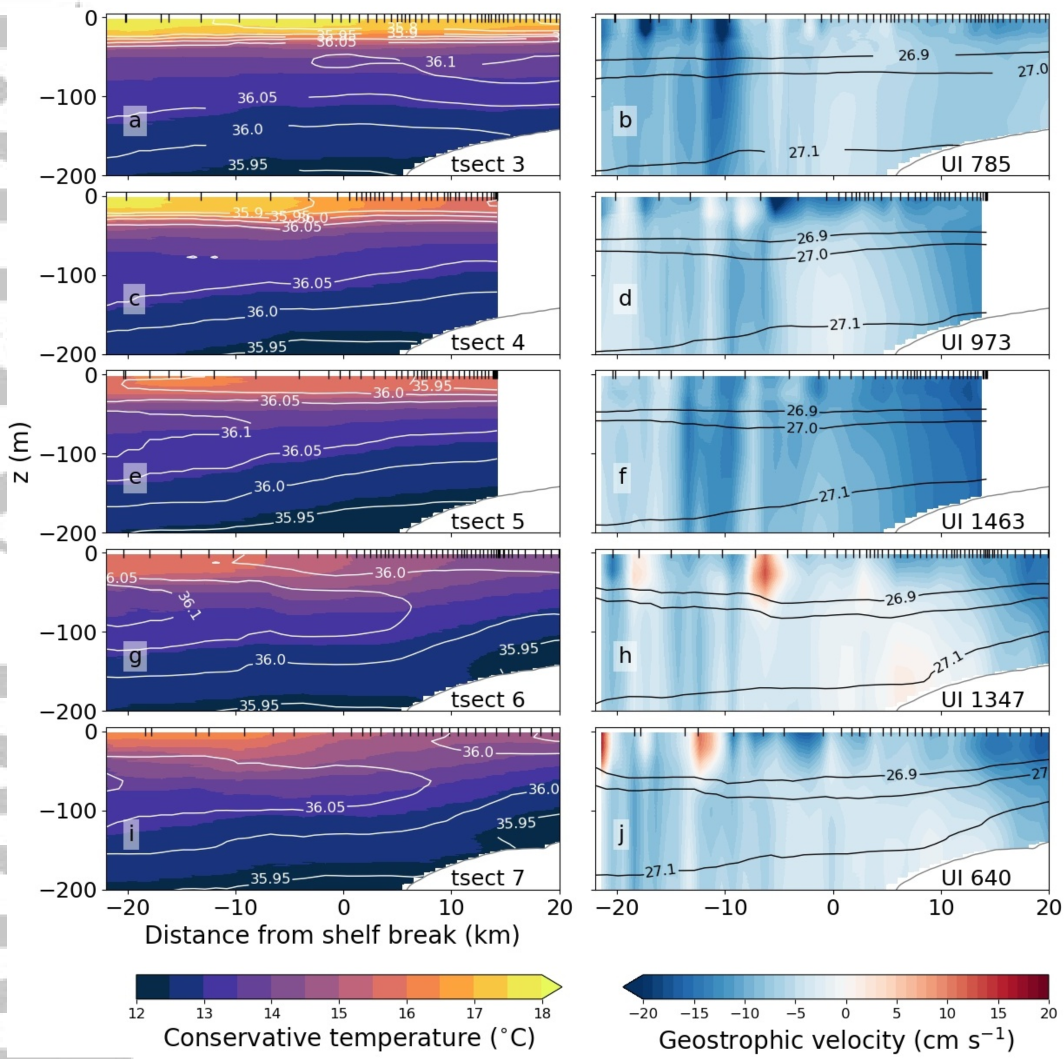

Figure 4. Evolution of conservative temperature (a,c,e,g,i) and meridional geostrophic velocity (b,d,f,h,j) during the first upwelling event, transects 3-7. (a,c,e,g,i) Contours are absolute salinity (g kg^{-1}). (b,d,f,h,j) Contours are density. UI on each figure in m^3 s^{-1} km^{-1} and is the value at the time the glider crossed the shelf break. Black ticks at the top of figures mark surfacings of the glider.

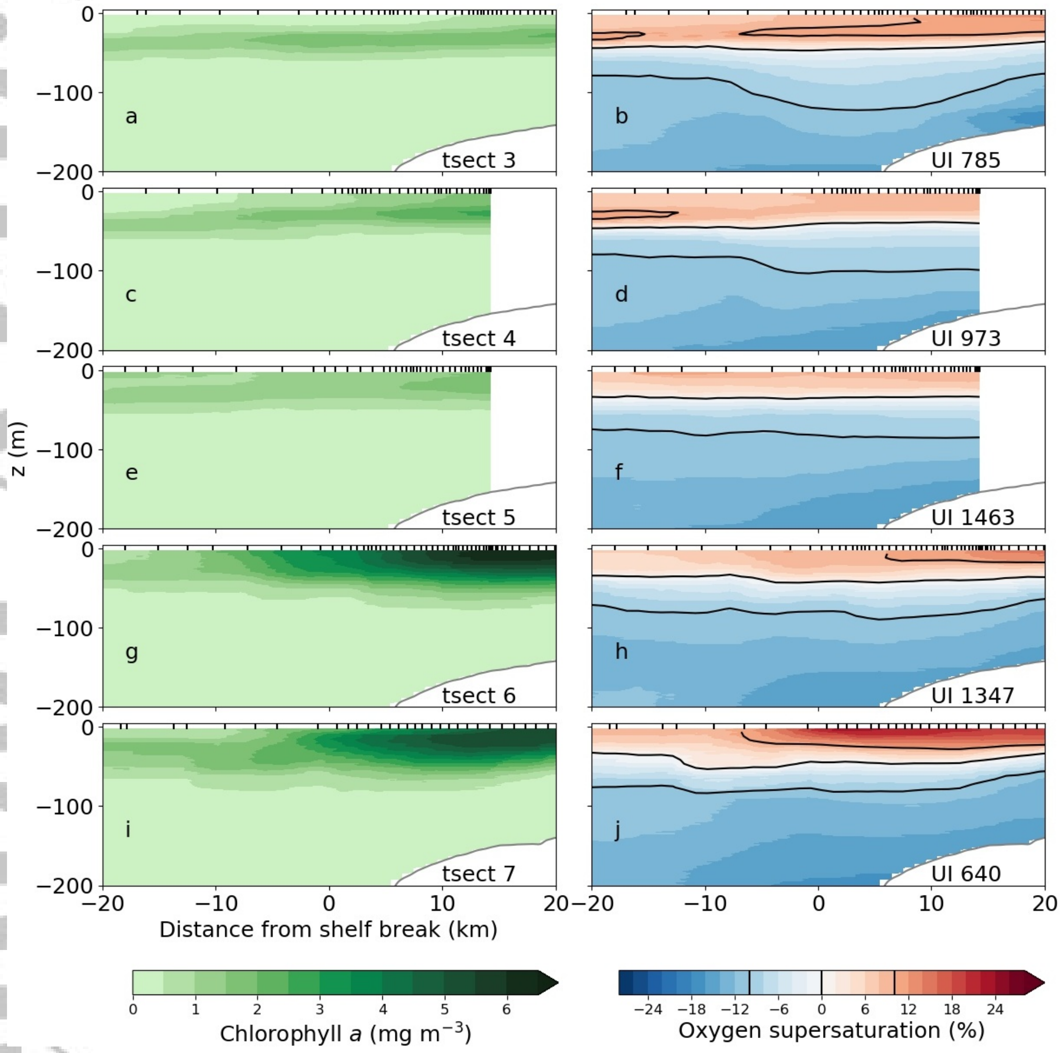

Figure 5. Evolution of chlorophyll *a* concentration (a,c,e,g,i) and oxygen supersaturation ($\Delta(O_2)$) (b,d,f,h,j). (b,d,f,h,j) -10, 0 and 10 % $\Delta(O_2)$ contours in black. Annotations as in Figure 4.

apparent in the increase in the equatorward current over the outer shelf from 3 to 8 cm s^{-1} during transect 4 (14 June, Figure 6a). The buoyant plume of water was advected 30 km offshore in 4 days (Figures 4a and 4c). The front between the warm water of the buoyant plume and cooler upwelled water moved offshore at approximately 0.1 m s^{-1}, consistent with previous observations of frontal advection during upwelling (Rossi et al., 2013). This current speed is comparable to that of the glider and prevented it from reaching its eastern waypoint on transect 4 (Figure 6). Because of this, we have no glider observations for the shelf more than 14 km inshore of the shelf break for 10 days. This period coincided with the wind speed peak of the first upwelling event. Satellite data show surface cooling and elevated chlorophyll *a* concentrations during this time period (Figures 6c and 7c).

After the offshore advection of the buoyant plume, near surface waters over the shelf became cooler and more saline (Figures 4g and 4i). Temperature near the surface decreased by as much as 3.0 °C at the eastern end of the section (Figure 6a). An across slope temperature gradient of 0.1 °C km^{-1} in the upper 20 m was observed (Figure 3b) typical of a front between warm surface and cool upwelled waters (Ferreira Cordeiro, 2018). Over the shelf, the $\sigma_\theta = 27.1$ kg m^{-3} isopycnal shoaled from 180 m to shallower than 100 m (Figures 4b and 4h). A core of cool, saline water with temperature-salinity characteristics between those of $ENACW_{st}$ and $ENACW_{sp}$ was upwelled onto the shelf during transects 6 and 7 (17-23 June, Figures 4g and 4i). The presence of this water on the shelf suggests upwelling of waters from depths of greater than 190 m, as has been observed previously (Huthnance et al., 2002). The change from near horizontal isopycnals pre-upwelling to isopycnal slopes of 4 m km^{-1} across the shelf break is pronounced (Figures 3c and 3d). The $\sigma_\theta = 27.0$ kg m^{-3} isopycnal shoaled by 20 m over the shelf, similar to that observed during summer 2009 by Ferreira Cordeiro et al. (2018). During the upwelling event, isopycnals outcropped over the shelf break (Figure 3f).

Prior to the first upwelling event, average chlorophyll concentrations were similar on the shelf and over the slope, though concentrations over the slope exhibited more variability (Figures 7 and 8a). Chlorophyll concentrations increased after the development of full upwelling, coincident with the decrease in near surface temperature (Figure 7). Higher chlorophyll concentrations were observed over the shelf than the slope for the entirety of the upper 100 m during transect 6 (Figure 8c). The subsurface chlorophyll maximum over the shelf shoaled to 12 m and near surface concentrations surpassed 6.0 mg m^{-3}

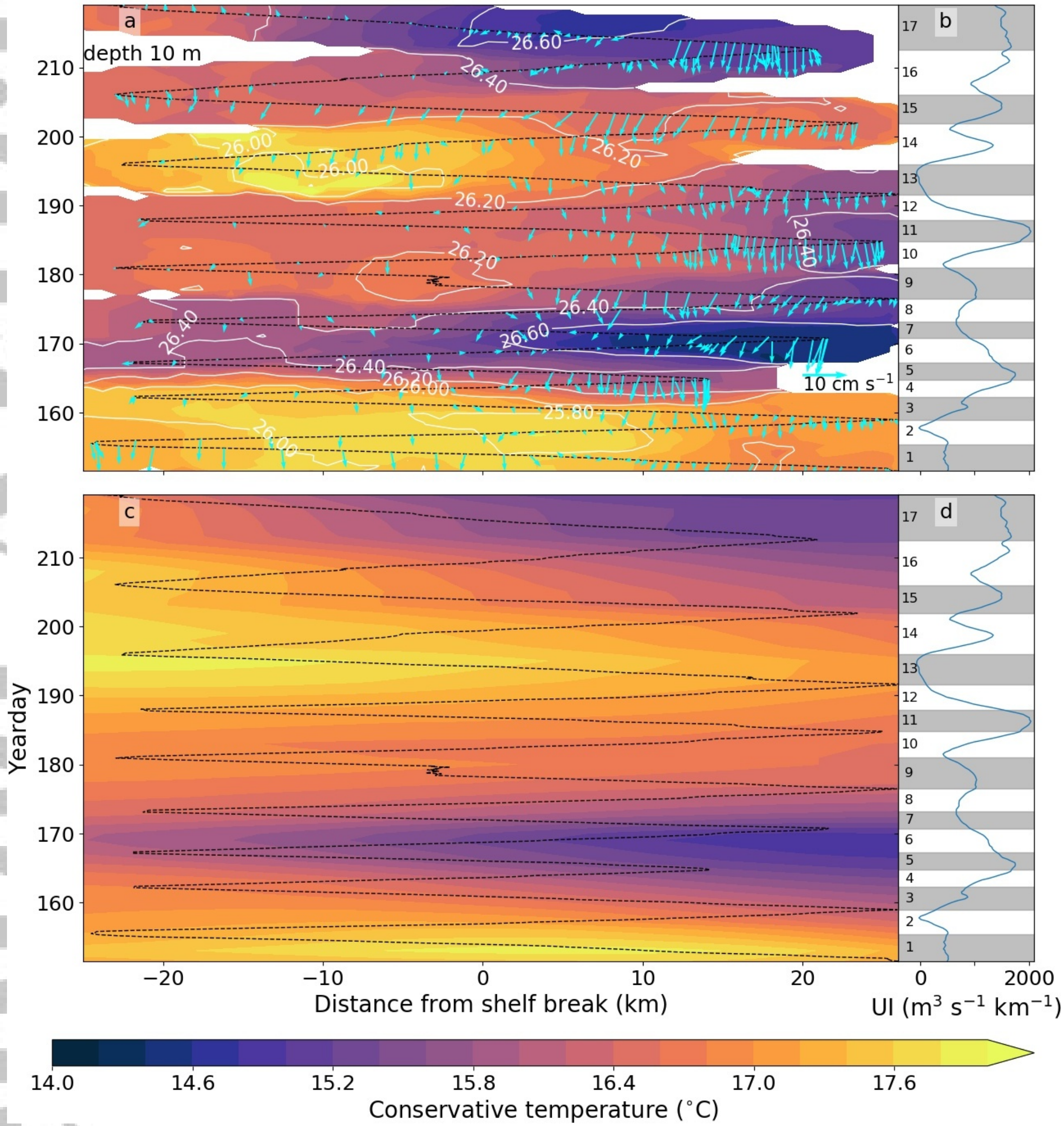

Figure 6. (a) Conservative temperature at 10 m depth. Black dashed line demarcates glider track in time. Black lines are potential density anomalies in kg m^{-3}. Cyan vectors are detided dive average currents. (c) Satellite observed SST with glider track overlaid. (b & d) Upwelling Index (UI) with glider transects shaded and numbered as in Figure 1.

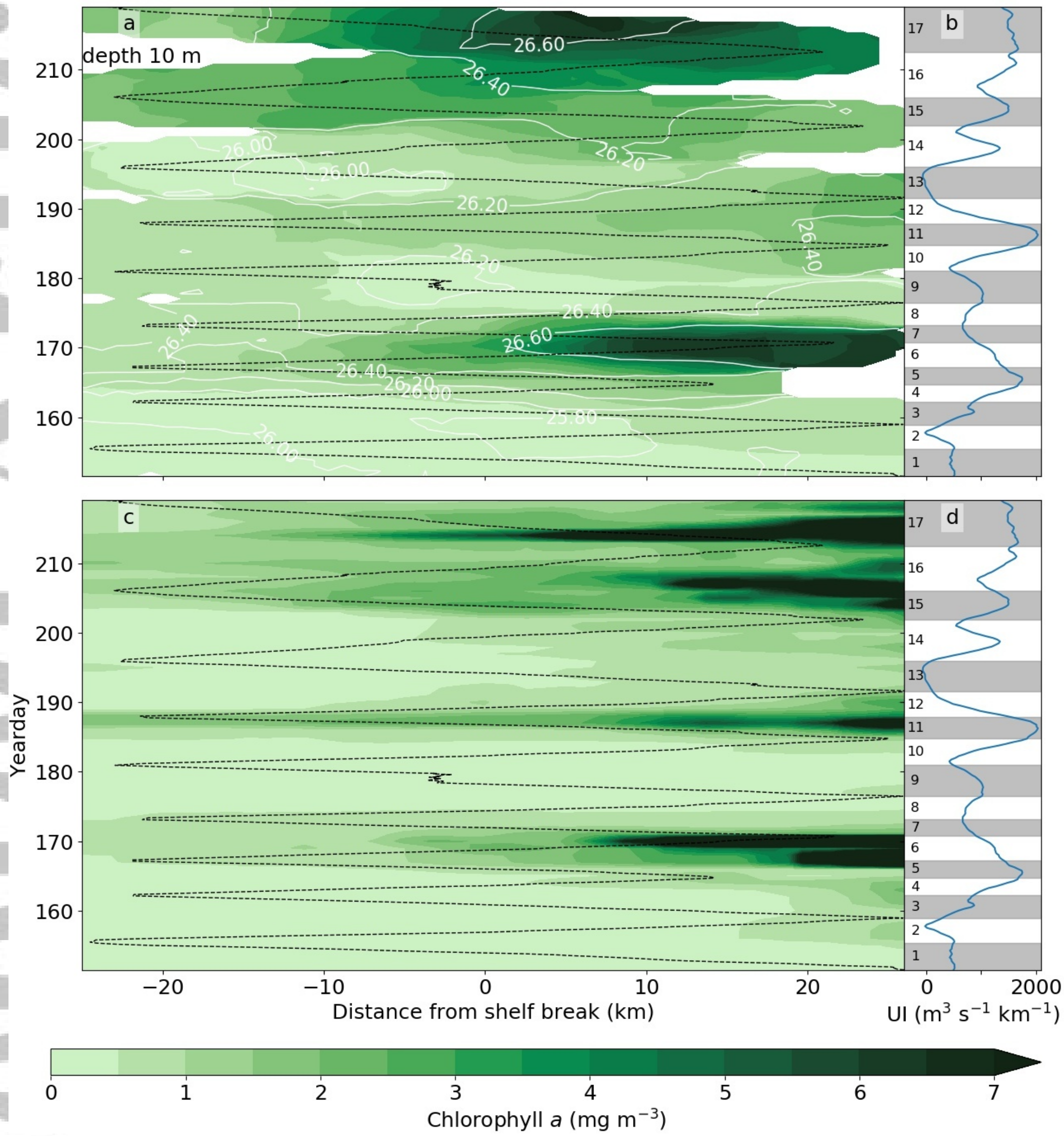

Figure 7. As Figure 6 for Chlorophyll *a* concentration.

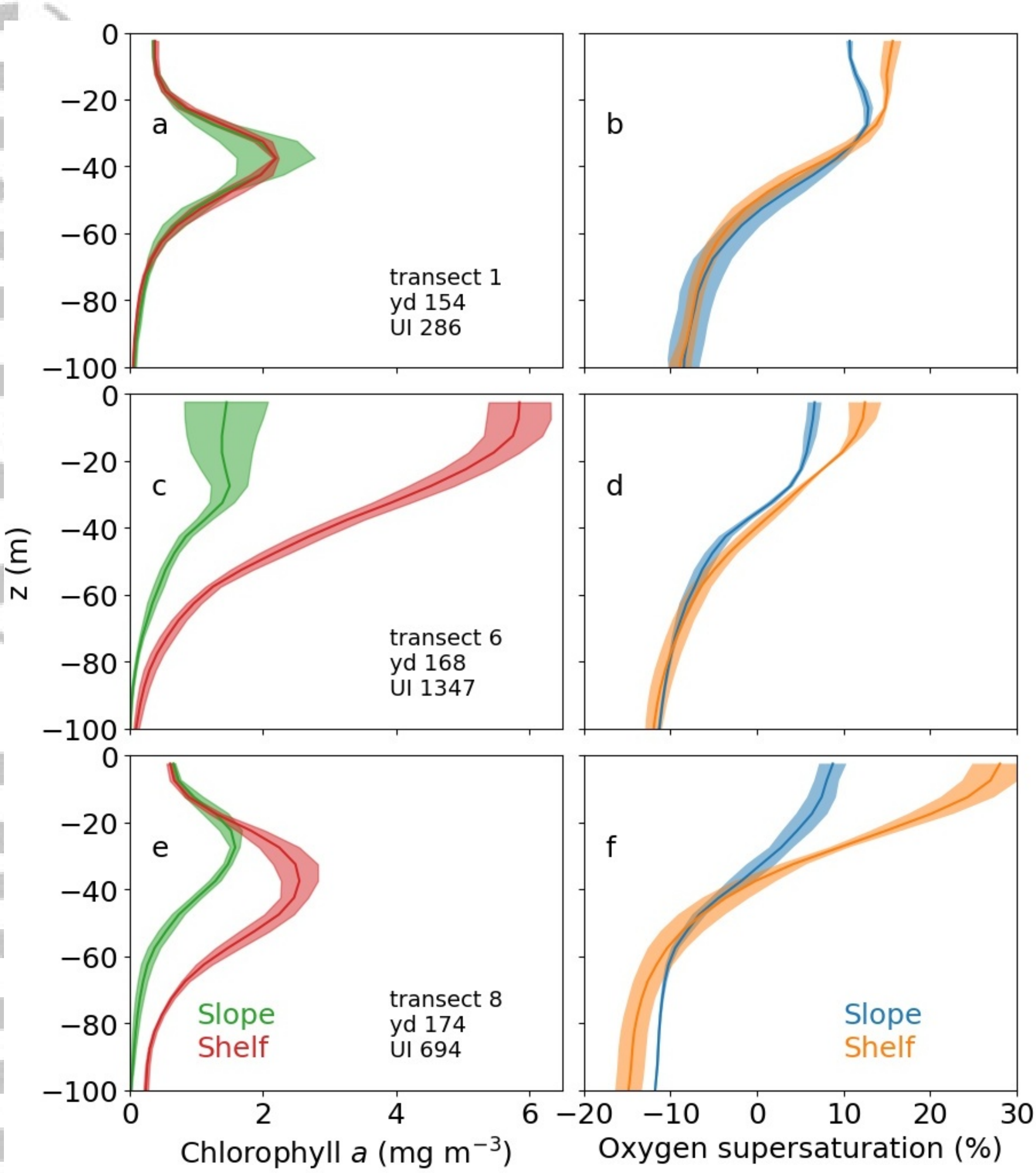

Figure 8. Mean vertical profiles of chlorophyll concentration (a,c,e) and $\Delta(O_2)$ (b,d,e) before and during the first upwelling event. The green and blue lines are the average of the water column over the slope, more than 5 km west of the shelf break. The red and orange lines are the average of the water column over the shelf, more than 5 km east of the shelf break. Uncertainty of 1 standard deviation is shaded around each profile. Transect number, yearday of the transect and UI during the transect are shown on each panel.

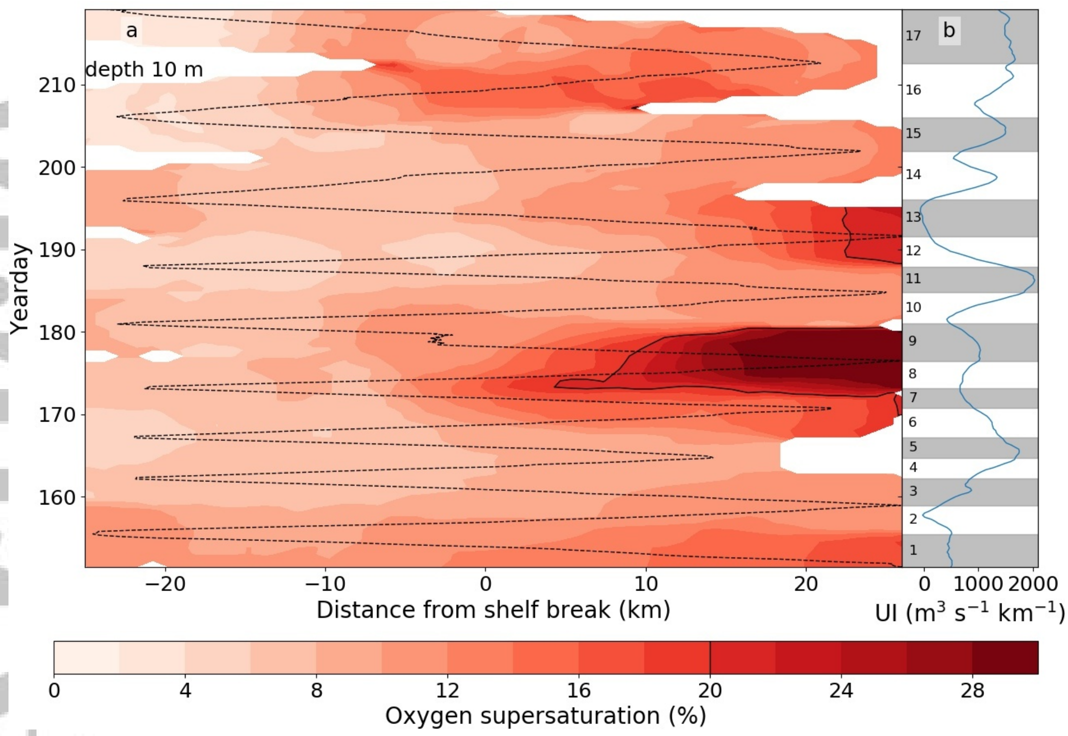

Figure 9. As Figure 6a and 6b for $\Delta(O_2)$. 20 % $\Delta(O_2)$ contour in solid black.

over the inner shelf more than 10 km inshore of the shelf break during transects 6-7 (Figure 7). $\Delta(O_2)$ followed the same pattern as chlorophyll but peaked during transects 8-9, 6 days later (Figures 7 and 9). $\Delta(O_2)$ increased most in the near surface over the shelf to greater than 28 %. during transect 8, the greatest supersaturation observed during the deployment (Figures 8f and 9). Chlorophyll and $\Delta(O_2)$ over the slope increased only slightly during the same time period (Figures 8c-8f).

After peaking during transect 7, maximum chlorophyll concentration over the shelf decreased to 2.3 mg m^{-3} and the subsurface chlorophyll maximum descended to 43 m during transects 8 and 9. $\Delta(O_2)$ over the shelf also decreased, reaching a minimum during transects 10 and 11, 8 days later than the minimum of chlorophyll in the near surface (Figures 7 and 9).

A brief period of strong equatorward wind around YD 188 (8 July, transects 10-11) increased equatorward current speed on the shelf (Figure 6a). However, this event was short lived and caused only a modest decrease in temperature on shelf at the eastern end of the transect (Figure 6a). Small increases in chlorophyll (0.5 mg m^{-3}) and $\Delta(O_2)$

(10 %) in the near surface were observed during the following transects 12-13 (Figures 7 and 9). The effects of this period of increased winds were mainly limited to the inner shelf, more than 10 km east of the shelf break (Figures 6, 7 and 9).

3.3 Partial relaxation and second upwelling event

A relaxation of the southward winds during YDs 191-194 (11-14 July, transect 13) brought surface warming of 2.0 °C over the slope and a decrease in the strength of equatorward flows (Figure 6). This relaxation was not sufficient to reverse the equatorward flow on the shelf, as has been observed during periods of northward winds in other years (Ferreira Cordeiro et al., 2018). Chlorophyll concentrations over the slope and shelf decreased (Figure 7).

During the final three transects of the deployment (21 July-8 August) a second upwelling event developed. This second event followed a similar pattern to the first with increased equatorward currents over the shelf and upwelling of cold, dense water decreasing near surface temperature by 2.0 °C (Figure 6). During the final transect, chlorophyll concentrations over the shelf increased to similar levels as observed during the first upwelling event (Figure 7). The highest chlorophyll concentration in the near surface were observed on the outer shelf at 5 km east of the shelf break (Figure 7). Assuming a similar lag between chlorophyll and $\Delta(O_2)$ in the near surface as observed during the first upwelling event, it is likely that $\Delta(O_2)$ increased past the end of the deployment.

3.4 Geostrophic currents and transports

As expected for the NWIM, along slope flows dominated, as shown by the DACs (Figure 6). During the deployment, the wind was primarily perpendicular to the glider transect, so Ekman flow contributed little to along slope velocities. After detiding and gridding (Section 2.2), we assume the velocity structure we observe to be dominated by geostrophic flow. The DACs include ageostrophic contributions from wind stress.

The alongshore flow averaged horizontally and vertically over the entire section, and over its shelf and slope subsections, was equatorward in every transect, even though poleward jets were present (Figure 6a). Average equatorward transport was 0.17 (± 0.07) Sv over the shelf and 0.83 (± 0.6) Sv over the slope. Averaged over the 17 transects (not shown) surface intensification of southward flow over the shelf is apparent, particularly at the near-shore end of the section, with a maximum flow speed of 15 cm s^{-1}. A minimum in southward flow speed of 2 cm s^{-1} was observed near the sea floor at the shelf break. Over the slope, equatorward flow is strongest at 50-150 m, the typical depth of $ENACW_{st}$. Equatorward flow weakens with depth, reaching a minimum flow speed below 700 m, at the depth of MEDW (Figure 3e and 3f).

During the 2 months of observation there was substantial variability in the strength of the equatorward transport. During upwelling, current speed increased over the shelf and the flow became more surface intensified (Figures 4d, 4f and 4h). Transport on the shelf increased from 0.13 (± 0.04) Sv to 0.18 (± 0.08) Sv during the two upwelling events. This flow is strongest at the near-shore end of the section (Figure 3f). The flow can be reasonably expected to extend further inshore, as has been observed in previous upwelling seasons on the NWIM (Rossi et al., 2013; Ferreira Cordeiro et al., 2018) and therefore our transport is likely an underestimate.

Over the slope, a broad equatorward flow dominated in the upper 500 m (Figure 3e). This flow was observed to weaken at depth, with a sporadic poleward flow below 500 m (Figure 3f). No relation was found between the UI and meridional transport over the slope. Opposing jet pairs were observed in the near surface throughout the deployment (Figures 4e and 4f). These moved offshore (westward) during the first upwelling event at 2 cm s^{-1}, similar to the upwelling event observed by Rossi et al. (2013).

4 Discussion

During June and July of 2010, the shelf and slope near Cape Silleiro experienced summer upwelling similar in character to that of previous years, but stronger (Relvas et al., 2007). In contrast to previous years, which featured cycles of upwelling and relaxation (Rossi et al., 2013; Ferreira Cordeiro et al., 2018), upwelling conditions dominated the observational period. A cross shore temperature gradient between cool upwelled water over the shelf and warmer surface waters offshore was present during the majority of the deployment (Figure 6). Isopycnal outcropping was frequently observed over the shelf and upper slope (Figure 4).

During the first upwelling event, mean temperature of the upper 20 m of the water column over the shelf decreased by 2.5 °C in less than 8 days (Figure 6). Latent heat loss to the atmosphere averaged 120 W m^{-2} during this period of increased wind speed (data from ERA5 Global Reanalysis (Copernicus Climate Change Service (C3S), 2017), not shown). Over 8 days this latent heat loss would cool the uppermost 20 m of the water column by 1.0°C. Sensible heat loss over the same period was an order of magnitude smaller. The cooling can only be the result of upwelled deeper water or horizontal advection of a temperature gradient. Previous studies have established upwelling as the mechanism by which cool, nutrient rich water reaches the near surface over the shelf (Relvas et al., 2007; Ferreira Cordeiro et al., 2018). Additionally, satellite SST data show that cool water features centred on the capes, including Cape Silleiro, expand and contract zonally but do not migrate meridionally (not shown). This is strongly indicative of upwelling, not advection. Surface cooling would not explain the observed changes in salinity, chlorophyll, $\Delta(O_2)$ and near surface currents which can only be the result of upwelling.

Upwelling raised the subsurface chlorophyll maximum and increased chlorophyll concentration throughout the mixed layer over the shelf and shelf break (Figure 8). The upwelled ENACW is relatively low in oxygen but the high nutrient concentration promotes phytoplankton growth (Rossi et al., 2013). We take elevated chlorophyll (Figure 7) and optical backscatter (not shown) to be indicators of elevated primary productivity and biomass, whilst acknowledging that processes such as photoacclimation or changes in pigment packaging and ecosystem composition can influence chlorophyll without necessarily increasing primary productivity and biomass (Cetinić et al., 2015). Increased primary productivity would account for the observed increase of $\Delta(O_2)$ (Figure 8). $\Delta(O_2)$ peaked after chlorophyll (and optical backscatter at 650 nm, not shown) over the shelf, with a delay of approximately 6 days. Oxygen in the mixed layer will also be affected by air-sea gas exchange, which will cause a further lag in the peak response of $c(O_2)$ with respect to the chlorophyll concentration. This measurable time delay is therefore an important result. Chlorophyll concentration provides a convoluted signal of productivity and biomass, whereas oxygen concentration is an integrated signal of production, giving cumulative net community production. One would therefore expect the integrated signal of oxygen to reach its maximum after the peak in chlorophyll, as is shown in our glider observations.

During crossings 12 and 13, the local maxima of chlorophyll and $\Delta(O_2)$ coincided (Figure 7 and Figure 9). This could indicate that another mechanism affects the concentration of oxygen in near surface waters. This could be a physical effect such as bubble injection, or a different ecosystem response to that which contributed to the delay between maxima in chlorophyll and $\Delta(O_2)$ observed after the first upwelling event. The absence of observed lag could also be a result of the relatively long transect sampling interval; the time between between crossings 12 and 14 over the inner shelf was 10 days. As is apparent in Figure 7c, chlorophyll over the inner shelf can increase and decrease in as little as 3 days.

During the first upwelling the chlorophyll maximum and near surface temperature minimum were observed at the eastern end of the section. During the second upwelling event, the chlorophyll maximum and near surface temperature minimum were observed 5 km east of the shelf break by the glider. The observations of minimum near surface temperature and maximum chlorophyll near the shelf break during the second upwelling event may be due to observational limitations. During the second upwelling event the glider was travelling slowly due to biofouling. The glider reached the shelf break more than a day after its final sampling of the inner shelf. Satellite SST and chlorophyll data support this interpretation (Figures 6c and 7c). The bloom initiating with the second upwelling event spread further offshore than the first bloom (Figures 7a and Figures 7c). Westward DACs over the outer shelf and shelf break may have contributed to this offshore spreading of chlorophyll (Figure 6a).

In deeper water (> 50 m) over the shelf, $\Delta(O_2)$ decreased during and after upwelling events (Figure 8). A potential cause is the advection of low oxygen $\mathrm{ENACW_{sp}}$ onto the shelf. The upwelling of $\mathrm{ENACW_{sp}}$ is visible in the temperature and density transects (Figure 3) in the shoaling of the $\sigma_\theta = 27.1$ kg m^{-3} isopycnal over the inner shelf. Biological activity also contributes to low oxygen values in deeper water (Rossi et al., 2013). During upwelling, nutrients depleted by near surface phytoplankton are replenished at depth by microbial remineralisation, consuming oxygen (Álvarez-Salgado et al., 1997; Rossi et al., 2013). Our observations of decreased $\Delta(O_2)$ below 50 m over the shelf agree with observations of near-bottom low-oxygen layers by Rossi et al. (2013).

The persistence of equatorward flow over the shelf throughout the deployment is atypical for the NWIM. Prior studies of the summer upwelling season have observed a reversion to poleward flow over the shelf during relaxation of equatorward winds (Peliz et al., 2002; Rossi et al., 2013; Ferreira Cordeiro et al., 2018). The absence of poleward flow over the shelf in our observations may be due to the time taken for the glider to return to the shelf. After the relaxation of the southward winds during YDs 191-194 (11-

14 July), the glider was not present again over the shelf until YD 199 (19 July Figure 6). Ferreira Cordeiro et al. (2018) noted poleward flows from a relaxation period of only 5 days of weak winds. The shelf could have experienced poleward flow during the 5 days that the glider was off the shelf. Alternatively, the dominance of upwelling favourable winds in summer 2010 may explain this absence of observed poleward flow (Figure 2). No downwelling events were observed during the deployment.

Geostrophic flows matched the typical upwelling season flow regime of NWIM, with a near-shore surface intensified upwelling jet and equatorward flow over the shelf break and upper slope (e.g. the schematic shown by Ferreira Cordeiro et al. (2018)). Our observed equatorward transport over the shelf 0.17 ($\pm$ 0.07) Sv is greater than the seasonal transport of 0.09 Sv for June and July from the numerical modelling study of (Teles-Machado et al., 2015). This is expected as the 0.09 Sv is based on a climatology of the years 1989-2008, which all had lower median values of UI than 2010 (Figure 2). Our observations of poleward flow near the seafloor over the shelf during upwelling (Figure 3f) are in agreement with previous studies observing a poleward countercurrent during upwelling at this location (Ferreira Cordeiro et al., 2018; Teles-Machado et al., 2015).

Offshore of the shelfbreak, a strong equatorward flow persisted throughout the deployment. We do not observe the poleward flow of the Iberian Poleward Current seen in models (Teles-Machado et al., 2015) and observations (Ferreira Cordeiro et al., 2018; Torres & Barton, 2007). This could be because the glider does not sample far enough offshore, turning around at 9.7 °W over bathymetry of 2000 m, midway down the slope (Figure 1). An observational campaign in June and July of 2009 only observed the poleward flow west of 9.8 °W (Ferreira Cordeiro et al., 2018). Earlier observational studies have shown a similar pattern of poleward flows in the upper 200 m west of 9.8 °W during the summer months (Torres & Barton, 2007). The observed pattern of equatorward flow dominance over the shelf and upper slope would be expected during upwelling conditions, with the upwelling jet keeping the IPC offshore as has been suggested by Nolasco et al. (2013).

The slow speed of the glider resulted in considerable time lapse between transects (6 days on average). Due to this, the glider did not observe some events apparent in the satellite chlorophyll data such as the increases in near surface chlorophyll concentration over the shelf YDs 188-190 and 205-208. The time gap between observations of the shelf limited our ability to constrain the timing of some events, such as the lag between the chlorophyll and $\Delta(O_2)$ maxima (Figures 7a and 9a). The strong currents over the shelf also prevented the glider from reaching its eastern waypoint during the development of the first upwelling event. The glider's short section limited our observations of along-shore currents over the deep slope and of upwelling features inshore of the 160 m isobath. Future glider deployments in the region will need to consider the trade off between section length and the frequency of observations at either end of the section. Alternatively, multiple gliders could be deployed concurrently.

5 Summary

An autonomous ocean glider was used to observe the 2010 summer upwelling season over the NWIM. Upwelling of cold ENACW from below 190 m contributed to an increase of near surface chlorophyll concentrations from less than 1 mg m^{-3} to greater than 7 mg m^{-3}. The increase in primary production contributed to a near surface increase of $\Delta(O_2)$ of 16 %, 6 days after the chlorophyll maximum. Decreasing $\Delta(O_2)$ was observed near the sea floor over the shelf during upwelling.

The 2010 summer upwelling season featured atypically strong upwelling favourable winds. Persistent net equatorward flow was observed on the shelf throughout the two month deployment, a phenomenon not previously observed. Equatorward flow increased and became more surface intensified during upwelling and a sporadic, weak poleward jet was observed over the shelf break.

This was the first, and to date only, deployment of a glider to observe summer upwelling over the NWIM. This study highlights some of the challenges of using gliders to study shelf break regions, particularly when the length of time between observations over the shelf is longer than the time period of current reversals on the shelf. Despite these difficulties, a single glider was able to occupy a cross shelf section for two months, without the need for a costly ship based campaign.

Acknowledgments

Glider data are held at the British Oceanographic Data Centre (Rollo et al., 2020), doi.org/10.5285/9b3b453b-2afb-0abd-e053-6c86abc0a59c. Wind speed and Upwelling Index and wind speed data were accessed from the Puertos del Estado database (Puertos del Estado, 2019) http://www.indicedeafloramiento.ieo.es/HBaixas/uitimeseries.ui. Bathymetry data from EMODnet Bathymetry Consortium (2018) doi.org/10.12770/18ff0d48-b203-4a65-94a9-5fd8b0ec35f6. Heat flux data from the ERA5 Global Reanalysis was accessed via the Copernicus Climate Change Service Information (Copernicus Climate Change Service (C3S), 2017) doi.org/10.24381/cds.bd0915c6. Sea surface fields from CMEMS Atlantic European North West Shelf Seas doi.org/10.5194/os-15-1133-2019. This study has been conducted using EU Copernicus Marine Service Information.

The glider deployment, and investigators JK and KJH, were supported by NERC grant NE/H012532/1. Ship work by the *RV Mytilus* was funded through the multidisciplinary project Canaries-Iberian Marine Ecosystem Exchanges (CAIBEX) (CTM2007-66408-C02-01/MAR)(Spanish Ministry of Education and Science). CR was supported by the Natural Environment Research Council (Grant NE/N012070/1) and the Engineering and Physical Sciences Research Council, via the NEXUSS Centre of Doctoral Training in the Smart and Autonomous Observation of the Environment.

We thank Liz Creed (formerly of iRobot, now at Hydroid) for her help during the deployment and piloting. We thank the crew and scientists of the *RV Mytilus* who made this deployment possible. Also thanks to the piloting team at UEA who kept the glider flying on UEA's first scientific glider mission.

The comments of three anonymous reviewers greatly enhanced this manuscript.

All plots were created with Python matplotlib (Hunter, 2007), Figure 1 also used cartopy (Met Office, 2010 - 2015). Filled contour plots used the cmocean perceptually uniform colourmaps developed by Thyng et al. (2016).

References

Alkire, M. B., D'Asaro, E., Lee, C., Perry, M. J., Gray, A., Cetinić, I., … González-Posada, A. (2012). Estimates of net community production and export using high-resolution, Lagrangian measurements of O2, NO3-, and POC through the evolution of a spring diatom bloom in the North Atlantic. *Deep Sea Research Part I: Oceanographic Research Papers*, *64*, 157–174. doi: 10.1016/j.dsr.2012.01.012

Álvarez-Salgado, X., Castro, C., Pérez, F., & Fraga, F. (1997). Nutrient mineralization patterns in shelf waters of the Western Iberian upwelling. *Continental*

Shelf Research, *17*(10), 1247–1270. doi: 10.1016/s0278-4343(97)00014-9

Álvarez-Salgado, X., Gago, J., Miguez, B., Gilcoto, M., & Pérez, F. (2000). Surface Waters of the NW Iberian Margin: Upwelling on the Shelf versus Outwelling of Upwelled Waters from the Rías Baixas. *Estuarine, Coastal and Shelf Science*, *51*(6), 821–837. doi: 10.1006/ecss.2000.0714

Arístegui, J., Barton, E. D., Álvarez-Salgado, X. A., Santos, A. M. P., Figueiras, F. G., Kifani, S., ... Demarcq, H. (2009). Sub-regional ecosystem variability in the Canary Current upwelling. *Progress in Oceanography*, *83*(1-4), 33–48. doi: 10.1016/j.pocean.2009.07.031

Barnes, S. L. (1994). Applications of the Barnes Objective Analysis Scheme. Part II: Improving Derivative Estimates. *Journal of Atmospheric and Oceanic Technology*, *11*(6), 1449–1458. doi: 10.1175/1520-0426(1994)011⟨1449:aotboa⟩2.0.co;2

Barton, E. (2001). Canary And Portugal Currents. In *Encyclopedia of ocean sciences* (pp. 380–389). Elsevier. doi: 10.1006/rwos.2001.0360

Brink, K. H. (1998). *The Sea, Vol. 10: The Global Coastal Ocean.* John Wiley and Sons.

Brown, C. W. (2013). *Seaglider observations of biogeochemical variability in the Iberian Upwelling System* (Doctoral dissertation, School of Envrionmental Sciences, University of East Anglia). Retrieved from `https://ueaeprints.uea.ac.uk/48788/`

Cetinić, I., Perry, M. J., D'saro, E., Briggs, N., Poulton, N., Sieracki, M. E., & Lee, C. M. (2015, April). A simple optical index shows spatial and temporal heterogeneity in phytoplankton community composition during the 2008 north atlantic bloom experiment. *Biogeosciences*, *12*(7), 2179–2194. doi: 10.5194/bg-12-2179-2015

Copernicus Climate Change Service (C3S). (2017). *ERA5: Fifth generation of ECMWF atmospheric reanalyses of the global climate accessed 29/05/2019.* Copernicus Climate Change Service Climate Data Store (CDS). Retrieved from `https://cds.climate.copernicus.eu`

Damerell, G. M., Heywood, K. J., Thompson, A. F., Binetti, U., & Kaiser, J. (2016). The vertical structure of upper ocean variability at the Porcupine Abyssal Plain during 2012-2013. *Journal of Geophysical Research: Oceans*, *121*(5), 3075–3089. doi: 10.1002/2015jc011423

Egbert, G. D., & Erofeeva, S. Y. (2002). Efficient inverse modeling of barotropic ocean tides. *Journal of Atmospheric and Oceanic Technology*, *19*(2), 183–204. doi: 10.1175/1520-0426(2002)019⟨0183:eimobo⟩2.0.co;2

EMODnet Bathymetry Consortium. (2018). *EMODnet Digital Bathymetry (DTM 2018)*. EMODnet Bathymetry Consortium. doi: 10.12770/18ff0d48-b203-4a65-94a9-5fd8b0ec35f6

Eriksen, C., Osse, T., Light, R., Wen, T., Lehman, T., Sabin, P., ... Chiodi, A. (2001). Seaglider: a long-range autonomous underwater vehicle for oceanographic research. *IEEE Journal of Oceanic Engineering*, *26*(4), 424–436. doi: 10.1109/48.972073

Ferreira Cordeiro, N. G. (2018). *Numerical and observational processes study of Northwestern Iberian margin circulation* (Doctoral dissertation, Departamento de Fisica, Universidade de Aveiro). Retrieved from `https://digital.csic.es/`

Ferreira Cordeiro, N. G., Dubert, J., Nolasco, R., & Barton, E. D. (2018). Transient response of the Northwestern Iberian upwelling regime. *PLOS ONE*, *13*(5). doi: 10.1371/journal.pone.0197627

Fiuza, A. F., Hamann, M., Ambar, I., del Rio, G. D., Gonzalez, N., & Cabanas, J. M. (1998). Water masses and their circulation off western Iberia during May 1993. *Deep Sea Research Part I: Oceanographic Research Papers*, *45*(7), 1127–1160. doi: 10.1016/s0967-0637(98)00008-9

Frajka-Williams, E., Eriksen, C. C., Rhines, P. B., & Harcourt, R. R. (2011). Determining Vertical Water Velocities from Seaglider. *Journal of Atmospheric and Oceanic Technology*, *28*(12), 1641-1656. doi: 10.1175/2011jtecho830.1

Garau, B., Ruiz, S., Zhang, W. G., Pascual, A., Heslop, E., Kerfoot, J., & Tintoré, J. (2011, September). Thermal Lag Correction on Slocum CTD Glider Data. *Journal of Atmospheric and Oceanic Technology*, *28*(9), 1065–1071. doi: 10.1175/jtech-d-10-05030.1

Garcia, H. E., & Gordon, L. I. (1992, September). Oxygen solubility in seawater: Better fitting equations. *Limnology and Oceanography*, *37*(6), 1307–1312. doi: 10.4319/lo.1992.37.6.1307

Garcia, H. E., & Gordon, L. I. (1993). Erratum: Oxygen solubility in seawater: Better fitting equations. *Limnology and Oceanography*, *38*(6), 656.

Hall, R. A., Aslam, T., & Huvenne, V. A. (2017). Partly standing internal tides in a dendritic submarine canyon observed by an ocean glider. *Deep Sea Research Part I: Oceanographic Research Papers*, *126*, 73–84. doi: 10.1016/j.dsr.2017.05.015

Herrera, J., Rosón, G., Varela, R., & Piedracoba, S. (2008). Variability of the western galician upwelling system (NW spain) during an intensively sampled annual cycle. an EOF analysis approach. *Journal of Marine Systems*, *72*(1-4), 200–217. Retrieved from `https://doi.org/10.1016/j.jmarsys.2007.07.007` doi: 10.1016/j.jmarsys.2007.07.007

Hu, C., Lee, Z., & Franz, B. (2012). Chlorophyll a algorithms for oligotrophic oceans: A novel approach based on three-band reflectance difference. *Journal of Geophysical Research: Oceans*, *117*(C1). doi: 10.1029/2011jc007395

Hunter, J. D. (2007). Matplotlib: A 2D Graphics Environment. *Computing in Science & Engineering*, *9*(3), 90–95. doi: 10.1109/mcse.2007.55

Huthnance, J. M., Aken, H. M. V., White, M., Barton, E., Cann, B. L., Coelho, E. F., ... Vitorino, J. (2002). Ocean margin exchange—water flux estimates. *Journal of Marine Systems*, *32*(1-3), 107–137. doi: 10.1016/s0924-7963(02)00034-9

IOC, S., & IAPSO. (2010). *The international thermodynamic equation of seawater 2010: Calculation and use of thermodynamic properties.* Intergovernmental Oceanographic Commission, Manuals and Guides no. 56.

Joint, I., Groom, S. B., Wollast, R., Chou, L., Tilstone, G. H., Figueiras, F. G., ... Smyth, T. J. (2002). The response of phytoplankton production to periodic upwelling and relaxation events at the iberian shelf break: estimates by the 14c method and by satellite remote sensing. *Journal of Marine Systems*, *32*(1-3), 219–238. doi: 10.1016/s0924-7963(02)00037-4

Maxwell, K., & Johnson, G. N. (2000). Chlorophyll fluorescence—a practical guide. *Journal of Experimental Botany*, *51*(345), 659–668. doi: 10.1093/jexbot/51.345.659

McClain, C. R., Chao, S.-Y., Atkinson, L. P., Blanton, J. O., & Castillejo, F. D. (1986). Wind-driven upwelling in the vicinity of Cape Finisterre, Spain. *Journal of Geophysical Research*, *91*(C7), 8470. doi: 10.1029/jc091ic07p08470

Merckelbach, L. M., Briggs, R. D., Smeed, D. A., & Griffiths, G. (2008). Current measurements from autonomous underwater gliders. In *2008 IEEE/OES 9th working conference on current measurement technology.* IEEE. doi: 10.1109/ccm.2008.4480845

Met Office. (2010 - 2015). Cartopy: a cartographic python library with a matplotlib interface [Computer software manual]. Exeter, Devon.

Nolasco, R., Pires, A. C., Cordeiro, N., Cann, B. L., & Dubert, J. (2013). A high-resolution modeling study of the Western Iberian Margin mean and seasonal upper ocean circulation. *Ocean Dynamics*, *63*(9-10), 1041–1062. doi: 10.1007/s10236-013-0647-8

Pauly, D., & Christensen, V. (1995). Primary production required to sustain global fisheries. *Nature*, *374*(6519), 255–257. doi: 10.1038/374255a0

Peliz, Á. (2003). Generation and unstable evolution of a density-driven eastern poleward current: The iberian poleward current. *Journal of Geophysical Research*, *108*(C8). Retrieved from https://doi.org/10.1029/2002jc001443 doi: 10.1029/2002jc001443

Peliz, Á., Rosa, T. L., Santos, A. P., & Pissarra, J. L. (2002). Fronts, jets, and counter-flows in the Western Iberian upwelling system. *Journal of Marine Systems*, *35*(1-2), 61–77. doi: 10.1016/s0924-7963(02)00076-3

Pietri, A., Testor, P., Echevin, V., Chaigneau, A., Mortier, L., Eldin, G., & Grados, C. (2013). Finescale Vertical Structure of the Upwelling System off Southern Peru as Observed from Glider Data. *Journal of Physical Oceanography*, *43*(3), 631–646. doi: 10.1175/jpo-d-12-035.1

Puertos del Estado. (2019). *Upwelling Index, Rias Baixes accessed 22/01/2019.* Puertos del Estado. Retrieved from http://www.indicedeafloramiento.ieo.es/HBaixas/uitimeseries.ui

Quaresma, L. S., & Pichon, A. (2013). Modelling the barotropic tide along the West-Iberian margin. *Journal of Marine Systems*, *109-110*, S3–S25. doi: 10.1016/j.jmarsys.2011.09.016

Queste, B. (2014). *Hydrographic observations of oxygen and related physical variables in the North Sea and western Ross Sea Polynya. Ph.D. thesis.* (Doctoral dissertation, School of Envrionmental Sciences, University of East Anglia). Retrieved from https://ueaeprints.uea.ac.uk/48678/

Relvas, P., Barton, E., Dubert, J., Oliveira, P. B., Peliz, Á., da Silva, J., & Santos,

A. M. P. (2007). Physical oceanography of the western Iberia ecosystem: Latest views and challenges. *Progress in Oceanography*, *74*(2-3), 149–173. doi: 10.1016/j.pocean.2007.04.021

Ríos, A. F., Pérez, F. F., & Fraga, F. (1992). Water masses in the upper and middle North Atlantic Ocean east of the Azores. *Deep Sea Research Part A. Oceanographic Research Papers*, *39*(3-4), 645–658. doi: 10.1016/0198-0149(92)90093-9

Rollo, C., Heywood, K. J., Hall, R. A., & Kaiser, J. (2020). *Physical and biogeochemical data from a Seaglider on an Eastwesterly transect across the shelf-break on the Northwest Iberian margin from June - August 2010.* British Oceanographic Data Centre, National Oceanography Centre, NERC, UK. Retrieved from https://www.bodc.ac.uk/data/published_data_library/catalogue/10.5285/9b3b453b-2afb-0abd-e053-6c86abc0a59c/ doi: 10.5285/9b3b453b-2afb-0abd-e053-6c86abc0a59c

Rossi, V., Garçon, V., Tassel, J., Romagnan, J.-B., Stemmann, L., Jourdin, F., ... Morel, Y. (2013). Cross-shelf variability in the Iberian Peninsula Upwelling System: Impact of a mesoscale filament. *Continental Shelf Research*, *59*, 97–114. doi: 10.1016/j.csr.2013.04.008

Sheehan, P. M. F., Berx, B., Gallego, A., Hall, R. A., Heywood, K. J., Hughes, S. L., & Queste, B. Y. (2018). Shelf sea tidal currents and mixing fronts determined from ocean glider observations. *Ocean Science*, *14*(2), 225–236. doi: 10.5194/os-14-225-2018

Teles-Machado, A., Peliz, Á., McWilliams, J. C., Couvelard, X., & Ambar, I. (2015). Circulation on the Northwestern Iberian Margin: Vertical structure and seasonality of the alongshore flows. *Progress in Oceanography*, *140*, 134–153. doi: 10.1016/j.pocean.2015.05.021

Thomalla, S. J., Moutier, W., Ryan-Keogh, T. J., Gregor, L., & Schütt, J. (2018). An optimized method for correcting fluorescence quenching using optical backscattering on autonomous platforms. *Limnology and Oceanography: Methods*, *16*(2), 132–144. doi: 10.1002/lom3.10234

Thyng, K., Greene, C., Hetland, R., Zimmerle, H., & DiMarco, S. (2016). True Colors of Oceanography: Guidelines for Effective and Accurate Colormap Selection. *Oceanography*, *29*(3), 9–13. doi: 10.5670/oceanog.2016.66

Todd, R. E., Rudnick, D. L., Mazloff, M. R., Davis, R. E., & Cornuelle, B. D. (2011). Poleward flows in the southern california current system: Glider observations and numerical simulation. *Journal of Geophysical Research*, *116*(C2). doi: 10.1029/2010jc006536

Torres, R., & Barton, E. (2007). Onset of the Iberian upwelling along the Galician coast. *Continental Shelf Research*, *27*(13), 1759–1778. doi: 10.1016/j.csr.2007.02.005

van Aken, H. M. (2000). The hydrography of the mid-latitude Northeast Atlantic Ocean. *Deep Sea Research Part I: Oceanographic Research Papers*, *47*(5), 789–824. doi: 10.1016/s0967-0637(99)00112-0